Gaussian random field models of aerogels

J. Quintanilla[a)]
Department of Mathematics, P.O. Box 311430, University of North Texas, Denton, Texas 76203

R. F. Reidy[b)]
Department of Materials Science, P.O. Box 305310, University of North Texas, Denton, Texas 76203

B. P. Gorman[c)] and D. W. Mueller[d)]
Department of Physics, P.O. Box 311427, University of North Texas, Denton, Texas 76203

(Received 4 November 2002; accepted 31 January 2003)

A model capable of predicting pore characteristics and rendering representative images of porous materials is described. A long-term goal is to discriminate between open and closed porosities. Aerogels are modeled by intersecting excursion sets of two independent Gaussian random fields. The parameters of these fields are obtained by matching small-angle neutron scattering data with the scattering function for the model. The chord-length probability density functions are then computed for the model, which contain partial clustering information for the aerogels. Visualizations of this model are performed and compared to electron microscopy images and gas adsorption pore size distributions. © *2003 American Institute of Physics.* [DOI: 10.1063/1.1563038]

I. INTRODUCTION

Small-angle neutron scattering (SANS) is a well-recognized investigative method to characterize material microstructure.[1] Many research efforts have employed SANS and small-angle x-ray scattering (SAXS) to characterize aerogel structures. These techniques have been applied to examine a range of length scales and to study changes in structure with respect to processing variables.[2–7]

In previous work, the base-catalyzed tetraethoxysilane aerogel system was studied using a polydispersed hard-sphere model.[8,9] However, visualizing realizations of this model can be problematic at best. Also, clustering information about this hard sphere model has yet to be analytically derived since the spheres of this model are not assumed to be in thermal equilibrium.[10,11]

This study examines the viability of a Gaussian random field (GRF) model for SANS characterization of aerogels. Previously, variants of the GRF model have been employed in the literature to study a variety of material systems, including aerogels,[12] foamed solids,[13] mass and surface fractals,[14] polymer blends,[15] sandstone,[16] cellular solids,[17] tungsten-silver composites,[18] heather incidence,[19] and sulphide ores.[20] Here we attempt to match the scattering data of aerogels to the scattering function for the GRF model by minimizing over several parameters. Clustering information may then be obtained by computing the chord-length density functions for the model. Also, realizations of the GRF model may be constructed to determine if it in fact bears a morphological resemblance to the aerogel.

In Sec. II, we describe the construction of the aerogels currently under investigation. In Sec. III, we list previously known results about the GRF model. The GRF model used here will rely on seven parameters; we discuss in Sec. IV the method by which these parameters are selected. Finally, in Sec. V, we show our results for the choices of these parameters and a three-dimensional realization of the GRF model. The chord-length density function for the GRF model is also found and compared with the gas-adsorption derived pore size distribution.

II. EXPERIMENTAL INFORMATION

Aerogels were synthesized from a tetraethoxysilane (TEOS) precursor in ethanol (4:1 ethanol/ TEOS ratio) using a base catalyst (0.1N NH_4OH [pH = 9.6] in a 4:1 catalyst/ TEOS ratio), forming a gel in 1 cm diameter vials at 23 °C. The sample was aged in the solvent for 3 days and supercritically dried in liquid CO_2. The physical and neutron transmission characteristics of the supercritically dried aerogel are noted in Table I. The transmission coefficient has been calculated as the ratio of sample transmission and empty beam transmission.

Experiments were conducted on the 30-m SANS instrument on neutron guide NG-7 at the NIST Center for Neutron Research. Detector distances of 1.2, 4, and 15.3 m were used to effectively examine a large range of length scales, and 5 Å neutrons were employed to resolve extremely small length scales.

Gas adsorption measurements to determine sample surface area and pore size distribution were conducted on a Quantachrome NOVA 2200 using nitrogen as an absorbate. The sample microstructure was imaged using transmission electron microscopy (JEOL 100cx). Small pieces of aerogel were crushed, dispersed ultrasonically in ethanol, and ultimately deposited on holey carbon-coated Cu grids.

Other aerogels modeled using this method are base-catalyzed tetramethoxysilane samples. These materials were of varied water to alkoxide ratios, solvent to alkoxide ratios,

[a)]Electronic mail: johnq@unt.edu
[b)]Electronic mail: reidy@unt.edu
[c)]Electronic mail: bgorman@unt.edu
[d)]Electronic mail: mueller@unt.edu

TABLE I. Sample size and neutron transmission coefficient for the SANS scattering experiment.

Sample	Sample thickness	Sample density (g/cm^3)	Transmission coefficient (sample/empty beam)
TEOS	0.62 cm	0.367	0.76

and *p*H. The scattering curves for these samples did not differ markedly, but they do offer an opportunity to study similar structures.

III. MODEL CHARACTERIZATION

In this section, we define a mathematical model for aerogels: the intersection of two excursion sets of independent Gaussian random fields. We also discuss various microstructure functions, defined for general random media, which have been explicitly computed for the GRF model. As we will show in Sec. V, this model captures the essential morphology of aerogels.

A. Gaussian random fields

We consider isotropic GRFs y so that each value $y(\mathbf{r})$ is a Gaussian random variable with mean 0 and variance 1. Such GRFs are completely characterized by the field-field covariance function

$$g(r)=\langle y(\mathbf{0})y(\mathbf{r})\rangle, \tag{1}$$

where $r=|\mathbf{r}|$. In this paper, we will use the covariance function

$$g(r)=\frac{e^{-r/\xi}-(r_c/\xi)e^{-r/r_c}}{1-(r_c/\xi)}\frac{\sin(2\pi r/d)}{2\pi r/d}. \tag{2}$$

This choice of covariance function has three parameters: a correlation length ξ, a domain scale d, and a cutoff scale r_c. These parameters allow considerable flexibility in the shape of $g(r)$, and so Eq. (2) has been used frequently in previous modeling work.[12,21,22]

Many techniques for generating realizations of Gaussian random fields in a cube with side T have been presented in the literature; see Ref. 23 and references therein. In this paper, we use a method which may be efficiently evaluated using a fast Fourier transform algorithm:[24]

$$y(\mathbf{r})=\sum_{l=-N}^{N}\sum_{m=-N}^{N}\sum_{n=-N}^{N}c_{lmn}\exp(i\mathbf{k}_{lmn}\cdot\mathbf{r}), \tag{3}$$

where

$$\mathbf{k}_{lmn}=\frac{2\pi}{T}(l\hat{\mathbf{x}}+m\hat{\mathbf{y}}+n\hat{\mathbf{z}}). \tag{4}$$

The random variables c_{lmn} are chosen so that y is real and isotropic with zero mean. This includes a stipulation that

$$\mathrm{Var}(\mathrm{Re}\,c_{lmn})=\mathrm{Var}(\mathrm{Im}\,c_{lmn})=\frac{1}{2}\rho(\mathbf{k}_{lmn})\left(\frac{2\pi}{T}\right)^2, \tag{5}$$

where $\rho(\mathbf{k})$ is the spectral density which depends only on $k=|\mathbf{k}|$. It can be shown that a random field defined in this manner has covariance function given by

$$g(r)=\int_0^\infty 4\pi k^2\rho(k)\frac{\sin kr}{kr}dk. \tag{6}$$

For the three-parameter covariance function of Eq. (2), the spectral density is given by

$$\rho(k)=\frac{d^4[q(\xi)-q(r_c)]}{\pi^2(\xi-r_c)}, \tag{7}$$

where

$$q(x)=\frac{x^4}{[d^2+x^2(kd-2\pi)^2][d^2+x^2(kd+2\pi)^2]}. \tag{8}$$

B. Two-cut model

The two-cut model is made by taking a certain excursion set of a Gaussian random field. That is, the solid phase is defined to be all values of $\mathbf{r}$ which satisfy

$$\alpha\leqslant y(\mathbf{r})\leqslant\beta \tag{9}$$

for some thresholds α and β, while all other values of $\mathbf{r}$ are assigned to the pore phase.

Many characterizations of the microstructure of the two-cut model have been obtained in the literature;[12] we summarize them here. First, the volume fraction ϕ of the solid phase is

$$\phi=\phi_\beta-\phi_\alpha, \tag{10}$$

where

$$\phi_\alpha=\frac{1}{\sqrt{2\pi}}\int_{-\infty}^{\alpha}e^{-t^2/2}dt=\frac{1}{2}+\frac{1}{2}\mathrm{erf}\frac{\alpha}{\sqrt{2}}. \tag{11}$$

The definition for ϕ_β is similar.

Second, the two-point phase probability function $S_2(r)$ is defined to be the probability that two points separated by a distance r both lie in the solid phase. This is known to be equal to

$$S_2(r)=\phi^2+\frac{1}{2\pi}\int_0^{g(r)}\frac{dt}{\sqrt{1-t^2}}\left[\exp\left(-\frac{\alpha^2}{1+t}\right)-2\exp\left(-\frac{\alpha^2-2\alpha\beta t+\beta^2}{2(1-t^2)}\right)+\exp\left(-\frac{\beta^2}{1+t}\right)\right]. \tag{12}$$

Third, for a line which passes through a random material, let n_c be the average number of times per unit length that the line crosses the interface between the pore and solid phases. From stereology, n_c is known to be half of the material's specific surface. For the two-cut model,[16]

$$n_c=\frac{\gamma}{\pi}[e^{-\alpha^2/2}+e^{-\beta^2/2}], \tag{13}$$

where $\gamma=\sqrt{-g''(0)}$. For the particular choice of g in Eq. (2), we have

$$\gamma = \sqrt{\frac{4\pi^2}{3d^2} + \frac{1}{r_c \xi}}. \tag{14}$$

A typographical error in Eq. (48) of Ref. 16 has been corrected in Eq. (13).

Fourth, the surface-void correlation function $S_c(r)$ gives the correlation for finding two points separated by a distance of r so that one point in the solid phase and a second point on the interface. Rigorous bounds on the fluid permeability[25] and trapping constant[26] of random materials have been found which depend on this function. For spherical systems, $S_c(r)$ is a special case of the canonical distribution function.[27,28] For the two-cut model,[16]

$$S_c(r) = f_{\beta\beta}(r) + f_{\beta\alpha}(r) - f_{\alpha\beta}(r) - f_{\alpha\alpha}(r), \tag{15}$$

where

$$\begin{aligned} f_{ab}(r) &= \frac{\gamma e^{-b^2/2}}{2\pi}\left(1 + \operatorname{erf}\left[\frac{\gamma\{a - bg(r)\}}{\sqrt{2G(r)}}\right]\right) - \frac{g'(r)}{2\pi\sqrt{1-g(r)^2}} \\ &\quad \times \exp\left(-\frac{a^2 - 2abg(r) + b^2}{2[1-g(r)^2]}\right) \\ &\quad \times \operatorname{erf}\left[\frac{a - bg(r)}{\sqrt{2G(r)}}\frac{g'(r)}{\sqrt{1-g(r)^2}}\right] \end{aligned} \tag{16}$$

and

$$G(r) = |\gamma^2[1-g(r)^2] - [g'(r)]^2|. \tag{17}$$

A typographical error in Eq. (51) of Ref. 16 has been corrected.

C. Intersection model

Many variants of the above excursion set model have been proposed in the literature. One such variant takes as the solid phase the intersection of two independently constructed two-cut models. Formally, if $y_1(\mathbf{r})$ and $y_2(\mathbf{r})$ are two independent Gaussian random fields, the solid phase is defined to be all $\mathbf{r}$ so that

$$\alpha \leqslant y_1(\mathbf{r}) \leqslant \beta$$

and

$$\alpha \leqslant y_2(\mathbf{r}) \leqslant \beta. \tag{18}$$

Open-cell microstructures typical of aerogels can be constructed using this intersection model, as shown in Sec. V.

We summarize below known microstructure characterizations of the intersection model. We use boldface to distinguish these characterizations with their analogues for the two-cut model:

$$\boldsymbol{\phi} = \phi^2 = (\phi_\beta - \phi_\alpha)^2, \tag{19}$$

$$\mathbf{n}_c = 2\phi n_c, \tag{20}$$

$$\mathbf{S}_2(r) = [S_2(r)]^2, \tag{21}$$

$$\mathbf{S}_c(r) = 2S_2(r)S_c(r). \tag{22}$$

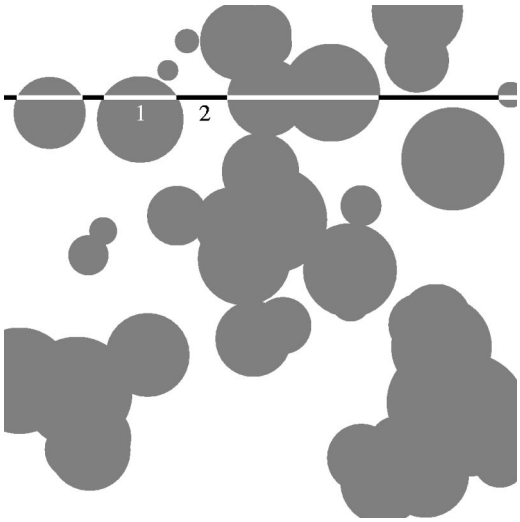

FIG. 1. A schematic depiction of the chords in a random medium. Because the chords measure length in a single direction, it is possible to get a large chord length through a narrow passageway.

D. Chord-length probability density function

An important characterization of random media is the chord-length probability density function.[11,28–30] If a line is drawn through a random material (as schematically illustrated in Fig. 1), the chords are defined to be the segments entirely in one phase with both end points on the interface. We define $p_1(r)$ and $p_2(r)$ to be the probability density functions of the chord lengths in phases 1 and 2, respectively.

The chord-length density function provides connectedness information about random materials, albeit in a single direction. This function is known to be proportional to the second derivative of the lineal path function or the probability of finding a line segment of given length completely within a certain phase. Both functions thus contain more information than $\mathbf{S_2}(r)$, which only requires that the end points of a line segment lie in a certain phase. Furthermore, this connectedness information can be used to accurately reconstruct random materials.[31–33]

Define

$$\hat{f}(s) = \int_0^\infty e^{-sr} f(r)\, dr \tag{23}$$

to be the Laplace transform of a function f. Roberts and Torquato found expressions for the Laplace transforms of the chord-length functions for both phases. For the intersection model,[16]

$$\hat{\mathbf{p}}_1(s) = \frac{\mathbf{n}_c - s[\hat{\mathbf{S}}_c(s) - s\hat{\mathbf{S}}_2(s) + \boldsymbol{\phi}]}{\mathbf{n}_c - s[\hat{\mathbf{S}}_c(s) + s\hat{\mathbf{S}}_2(s) - \boldsymbol{\phi}]} \tag{24}$$

and

$$\hat{\mathbf{p}}_2(s) = \frac{\hat{\mathbf{S}}_c(s) + s\hat{\mathbf{S}}_2(s) - \boldsymbol{\phi}}{\hat{\mathbf{S}}_c(s) - s\hat{\mathbf{S}}_2(s) + \boldsymbol{\phi}}. \tag{25}$$

Strictly speaking, these expressions are valid if the chord lengths are independent, an assumption that is not valid for

any GRF model. However, Roberts and Torquato also showed numerically that the dependence of the chord lengths minimally affects $\hat{\mathbf{p}}_1$ and $\hat{\mathbf{p}}_2$.

To find the original functions $\mathbf{p}_1(r)$ and $\mathbf{p}_2(r)$, we will use a short algorithm discovered by Abate and Whitt.[34,35] Based on previous experience,[16,30] evaluating the integrals which determine $\hat{\mathbf{p}}_1(s)$ and $\hat{\mathbf{p}}_2(s)$ to 10 or 11 decimal places will produce values of $\mathbf{p}_1(r)$ and $\mathbf{p}_2(r)$ accurate to roughly 3 or 4 decimal places.

It has been shown that $\mathbf{p}_1(r)$ and $\mathbf{p}_2(r)$ specify the small-angle scattering intensity.[36] In the next section, we take up the inverse problem: how to use scattering data to find an excursion set model for aerogels, from which chord-length data is obtained.

IV. FITTING INTERSECTION MODELS TO AEROGELS

In the previous section, we defined the intersection model of two independent isotropic Gaussian random fields. We will loosely follow a method of Roberts[12] to fit this model to the aerogels described in Sec. II. This will be done using neutron scattering information. Theoretically, the scattering intensity is given by[37]

$$I(k) = I_0 + V\eta^2 \int_0^\infty 4\pi r^2 [\mathbf{S}_2(r) - \boldsymbol{\phi}^2] \frac{\sin kr}{kr} dr, \tag{26}$$

where I_0 is background noise, V is the volume of the material, and η is the scattering density of the solid phase. In principle, given the intensity function, the two-point phase probability function may be computed using the inverse Fourier sine transformation:

$$\mathbf{S}_2(r) = \boldsymbol{\phi}^2 + \frac{1}{2\pi^2 V\eta^2} \int_0^\infty [I(k) - I_0] k^2 \frac{\sin kr}{kr} dk. \tag{27}$$

However, in practice, this is problematic since $I(k)$ can be measured only for finitely many wavenumbers k, and these measurements are subject to experimental error. As a result, there is no guarantee that the autocovariance function $\mathbf{S}_2(r) - \boldsymbol{\phi}^2$ will satisfy the theoretical requirement of positive semidefiniteness.

Instead of using the inversion formula (27), we attempt to match the experimentally measured intensity with the intensity curve predicted for the intersection model using Eqs. (12), (21), and (26). To determine the constant $V\eta^2$, we recall from scattering theory that the asymptotic form of the intensity function is given by[38]

$$I(k) \sim I_0 + \frac{a}{k^4}, \quad k \to \infty, \tag{28}$$

where the first nontrivial coefficient is given by

$$a = 4\pi\eta^2 \mathbf{n}_c V. \tag{29}$$

Therefore,

$$V\eta^2 = \frac{a}{4\pi \mathbf{n}_c}. \tag{30}$$

Since $\mathbf{n}_c$ is known for the model via Eq. (20), it remains to measure the first nontrivial term of the expansion (28). This may be done by a direct fit of the scattering data; however, such an approach is hampered by experimental limitations. Instead, we have chosen to treat a as a parameter to be fitted.

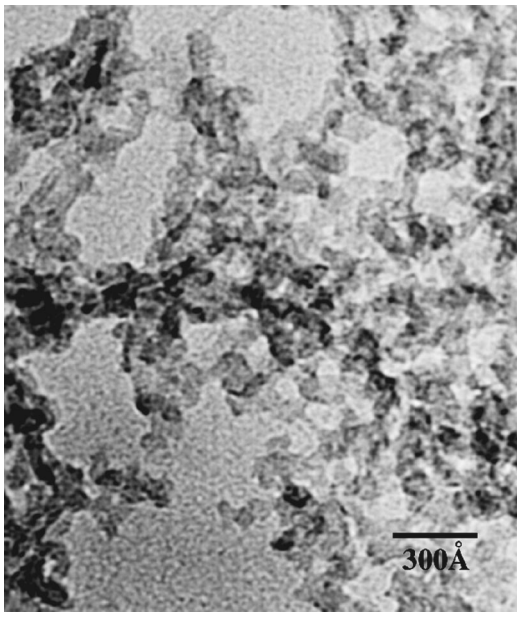

FIG. 2. Transmission electron microscopy image of TEOS.

In summary, we must attempt to match the scattering data of the aerogels to the model scattering function by optimizing over seven parameters: (i) the covariance function parameters ξ, d, and r_c, (ii) the thresholds α and β (or, equivalently, the volume fractions ϕ_α and ϕ_β), (iii) the coefficient a, and (iv) the background noise I_0.

This optimization is performed by minimizing the difference between the scattering data and the GRF model's scattering function using a least-squares method. Once the appropriate intersection model is found, realizations of the model may be constructed using the algorithm of Eq. (3) to determine if in fact the model bears a morphological resemblance to the aerogel. Furthermore, the chord-length density function for both phases of the model can be computed by numerically inverting Eqs. (24) and (25).

V. RESULTS

Figure 2 is a TEM image of the base-catalyzed TEOS aerogel. A loosely connected microstructure and spheroidal shape of the primary particles are evident. This sample is the result of fracture and an ethanol suspension prior to adding to the carbon grid; therefore, the three-dimensional character of the bulk aerogel may be somewhat different. Using the algorithm described in the previous section, we find that this aerogel is best modeled with the parameters $\xi = 53.744$ Å, $r_c = 53.743$ Å, $d = 249.146$ Å, $\phi_\alpha = 0.082\,43$, $\phi_\beta = 0.360\,14$, $a = 0.000\,119\,28$, and $I_0 = 0.035\,031\,3$.

We now discuss in detail the model used to find the TEOS data. In Fig. 3, we compare the SANS data for TEOS with the intensity curve computed using Eq. (26) and these seven parameters. As we see, the two curves appear to be in good agreement, especially in the important region of large k. A realization of this model (with dimensions 1500×1500

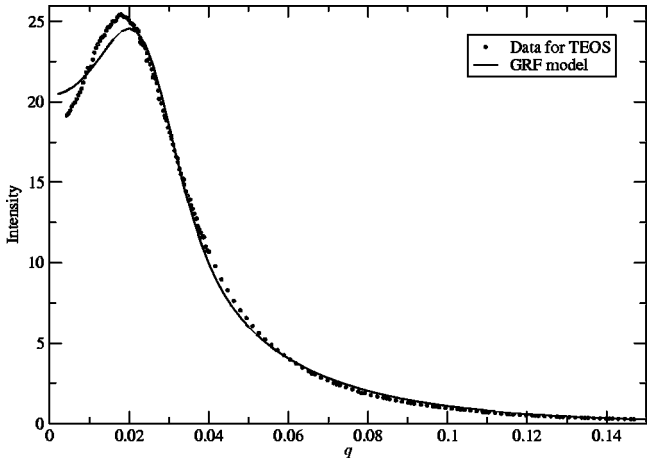

FIG. 3. The intensity curve for the intersection model and the experimental scattering data for TEOS.

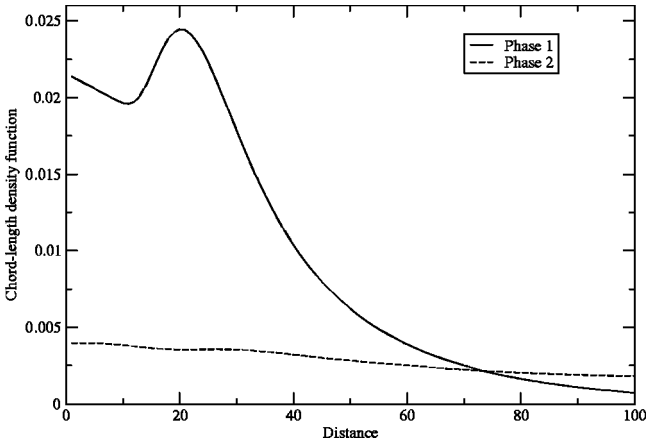

FIG. 5. The chord-length probability density functions for both phases of the intersection model for TEOS. For the solid phase, we find that $\boldsymbol{\mu}_1 = 28$ Å and $\boldsymbol{\sigma}_1 = 23$ Å, while $\boldsymbol{\mu}_2 = 334$ Å and $\boldsymbol{\sigma}_2 = 345$ Å for the pore phase.

$\times 187.5$ Å^3) is shown in Fig. 4. Most of the ''islands'' in the realization are actually connected to the rest of the solid phase outside of the region shown. This model is morphologically similar to the TEM images of TEOS of Fig. 2.

The chord-length density probability functions for the two phases are shown in Figs. 5 and 6. We notice that the chords of the solid phase are much shorter than the chords for the pore phase. We also observe that the chords in the solid phase tend to have lengths between 0 and 30 Å, with a peak around 20 Å. The average $\boldsymbol{\mu}_i$ and standard deviation $\boldsymbol{\sigma}_i$ of the chord lengths for both phases may be found through the formulas

$$\boldsymbol{\mu}_i = \int_0^\infty t \mathbf{p}_i(t) dt \tag{31}$$

and

$$\boldsymbol{\sigma}_i^2 = \left(\int_0^\infty t^2 \mathbf{p}_i(t) dt \right) - \mu_i^2 . \tag{32}$$

Using these equations, we find that $\boldsymbol{\mu}_1 = 28$ Å and $\boldsymbol{\sigma}_1 = 23$ Å for the solid phase, while $\boldsymbol{\mu}_2 = 334$ Å and $\boldsymbol{\sigma}_2 = 345$ Å for the pore phase.

Figure 7 describes the pore size distribution for the base-catalyzed TEOS sample. The peak fit suggests a Gaussian distribution while additional small peaks may reside in the 60–100 Å regime. In either case, the highest pore volume exists for peaks of approximately 120 Å. The calculated average pore size is 158 Å based on the BJH model.[39] This value compares well electron microscopy images in Fig. 2.

This average pore size is about half the size of the average chord length for the pore phase. This is to be expected from geometrical considerations: the average pore size measures the pore phase in all directions simultaneously, while the average chord length measures the pore phase in a single direction. For example, for systems of fully penetrable spheres with 88% porosity, the average distance between particles is known analytically to be about 6 times smaller than the average chord length.[28]

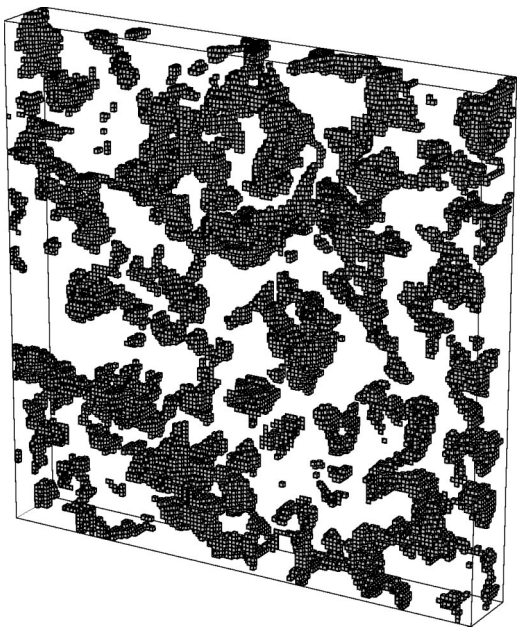

FIG. 4. A realization of the intersection model for TEOS. The dimensions of this realization are $1500 \times 1500 \times 187.5$Å^3.

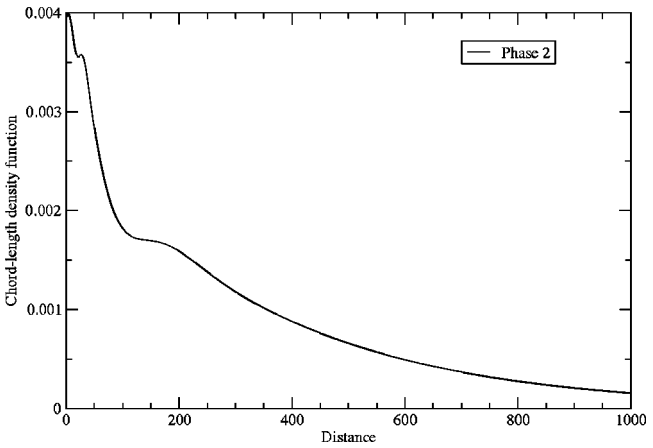

FIG. 6. As in Fig. 5 for the pore phase, except for distances up to 1000 Å.

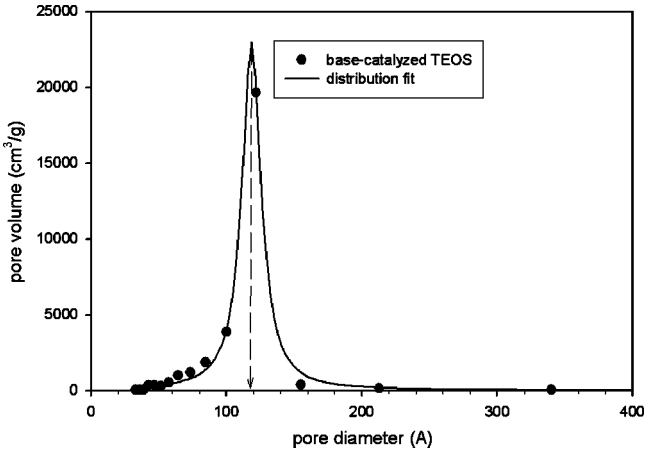

FIG. 7. The pore size distribution for the base-catalyzed TEOS sample. The most likely pore size is approximately 120 Å; the calculated average pore size of 158 Å is based on the Barrett–Joyner–Halenda (BJH) model.

In conclusion, this paper has studied intersections of Gaussian random fields as a potential model for aerogels. Realizations of this model bear a morphological resemblance to TEOS, and the theoretical intensity curve for the model closely matches the experimentally derived intensity curve for the aerogel. The analytic nature of the model lends itself to statistical testing; in future work, the researchers will study statistical techniques for validating this approach for modeling aerogels.

ACKNOWLEDGMENT

The authors thank Tony Roberts for the use of his code for simulating the excursion sets of Gaussian random fields.

[1] G. G. Long, S. Krueger, P. R. Jermain, D. R. Black, H. E. Burdette, J. P. Cline;, and R. A. Gerhardt, J. Appl. Crystallogr. **23**, 535 (1990).
[2] D. W. Hua, J. Anderson, S. Hereid, D. M. Smith, and G. Beaucage, Mater. Res. Soc. Symp. Proc. **346**, 985 (1994).
[3] J. Wang, J. Shen, B. Zhou, and X. Wu, Nanostruct. Mater. **7**, 699 (1996).
[4] D. W. Schaeffer, C. J. Brinker, J. P. Wilcoxon, D. Q. Wu, J. C. Phillips, and B. Chu, Mater. Res. Soc. Symp. Proc. **121**, 691 (1988).
[5] A. B. Jarzebski, J. Lorenc, and L. Pajak, Langmuir **13**, 1280 (1997).
[6] J. Mrowiec-Bialon, L. Pajak, A. B. Jarzebski, A. I. Lachowski, and J. J. Malinowski, Langmuir **13**, 6310 (1997).
[7] J. Hyeon-Lee, G. Beaucage, S. E. Prantsinis, and S. Vemury, Langmuir **14**, 5751 (1998).
[8] A. J. Allen, S. Krueger, G. Skandan, G. G. Long, H. Hahn, H. M. Kerch, J. C. Parker, and M. N. Ali, J. Am. Ceram. Soc. **79**, 1201 (1996).
[9] R. F. Reidy, A. J. Allen, and S. Krueger, J. Non-Cryst. Solids **285**, 181 (2001).
[10] B. L. Lu and S. Torquato, Phys. Rev. A **45**, 7292 (1992).
[11] S. Torquato and B. Lu, Phys. Rev. E **47**, 2950 (1993).
[12] A. P. Roberts, Phys. Rev. E **55**, R1286 (1997).
[13] A. P. Roberts and M. A. Knackstedt, J. Mater. Sci. Lett. **14**, 1357 (1995).
[14] A. P. Roberts and M. A. Knackstedt, Physica A **233**, 848 (1996).
[15] M. A. Knackstedt and A. P. Roberts, Macromolecules **29**, 1369 (1996).
[16] A. P. Roberts and S. Torquato, Phys. Rev. E **59**, 4953 (1999).
[17] A. P. Roberts and E. J. Garboczi, Acta Mater. **49**, 189 (2001).
[18] A. P. Roberts and E. J. Garboczi, J. Mech. Phys. Solids **47**, 2029 (1999).
[19] D. J. Nott and T. Rydén, Biometrika **86**, 661 (1999).
[20] D. J. Nott and R. J. Wilson, Signal Process. **80**, 125 (2000).
[21] S. Marčelja, J. Phys. Chem. **94**, 7259 (1990).
[22] M. Teubner and R. Strey, J. Chem. Phys. **87**, 3195 (1987).
[23] A. T. A. Wood and G. Chan, J. Comput. Graph. Stat. **3**, 409 (1994).
[24] A. P. Roberts, Phys. Rev. E **56**, 3203 (1997).
[25] J. Rubinstein and S. Torquato, J. Fluid Mech. **206**, 25 (1989).
[26] J. Rubinstein and S. Torquato, J. Chem. Phys. **88**, 6273 (1988).
[27] J. Quintanilla, Polym. Eng. Sci. **39**, 559 (1999).
[28] S. Torquato, *Random Heterogeneous Materials: Microstructure and Macroscopic Properties* (Addison-Wesley, New York, 2002).
[29] G. Matheron, *Random Sets and Integral Geometry* (Wiley, New York, 1975).
[30] J. Quintanilla and S. Torquato, Phys. Rev. E **54**, 4027 (1996).
[31] C. L. Y. Yeong and S. Torquato, Phys. Rev. E **57**, 495 (1998).
[32] C. L. Y. Yeong and S. Torquato, Phys. Rev. E **58**, 224 (1998).
[33] D. Cule and S. Torquato, J. Appl. Phys. **86**, 3428 (1999).
[34] J. Abate and W. Whitt, Queueing Syst. **10**, 5 (1992).
[35] J. Abate and W. Whitt, ORSA J. Comput. **7**, 36 (1995).
[36] P. Levitz and D. Tchoubar, J. Phys. I **2**, 771 (1992).
[37] A. Guinier, G. Fournet, C. B. Walker, and K. L. Yudowitch, *Small-angle Scattering of X-rays* (Wiley, New York, 1955).
[38] P. Debye, H. R. Anderson, Jr., and H. Brumberger, J. Appl. Phys. **28**, 679 (1957).
[39] E. P. Barrett, L. G. Joyner, and P. P. Halenda, J. Am. Chem. Soc. **73**, 373 (1951).